crystals

MDPI

Article

Simulation and Analysis of Single-Mode Microring Resonators in Lithium Niobate Thin Films

Huangpu Han [1,2], Bingxi Xiang [3,4,*] and Jiali Zhang [5]

1 College of Electric and Electronic Engineering, Zibo Vocational Institute, Zibo 255314, China; pupuhan@126.com
2 School of Physics, Shandong University, Jinan 250100, China
3 College of New Materials and New Energies, Shenzhen Technology University, Shenzhen 518118, China
4 Shenzhen Key Laboratory of Laser Engineering, College of Optoelectronic Engineering, Shenzhen University, Shenzhen 518060, China
5 College of General Education, Weifang University of Science and Technology, Weifang 262700, China; jialigg@126.com
* Correspondence: xiangbingxi@sztu.edu.cn; Tel.: +86-135-3085-0236

Received: 4 August 2018; Accepted: 22 August 2018; Published: 24 August 2018

check for updates

Abstract: The single-mode microring resonators on lithium niobate thin films were designed and simulated using 2.5-D variational finite difference time domain mode simulations from Lumerical mode Solutions. The single-mode conditions and the propagation losses of lithium niobate planar waveguide with different SiO_2 cladding layer thicknesses were studied and compared systematically. The optimization of design parameters such as radii of microrings and gap sizes between channel and ring waveguides were determined. The key issues affecting the resonator design such as free spectral range and Quality Factor were discussed. The microring resonators had radius R = 20 μm, and their transmission spectrum had been tuned using the electro-optical effect.

Keywords: microring resonator; integrated photonic; varfdtd; electro-optical; LNOI

1. Introduction

Lithium niobate ($LiNO_3$, LN) is one of the most promising materials because of its excellent electro-optical, piezoelectric, pyroelectric, photo-elastic and non-linear properties [1]. Due to the high electro-optical coefficient (γ_{33} = 31.2 pm/V) in LN, highly efficient electro-optical modulator in such material is very promising and always an interesting topic in optical interconnect technology [2]. In last ten years, high-refractive-index contrast, which is LN thin film on a low refractive index SiO_2 cladding layer or other substrates (lithium niobate on insulator, LNOI) has emerged, as it is compatible with the silicon on insulator (SOI) manufacturing technology [3]. LNOI is an interesting platform for integrated photonics due to the good confinement and strong guiding of light [4].

The microring resonator is one of the important elements in integrated photonic systems. Optical microring resonators are the promising candidates for a variety of applications, including wavelength filtering, multiplexing, switching and modulation [5–7]. The basic structure of the microring resonator consists of a channel and a ring. The microring resonators have been designed on various types of materials such as silicon [8], germanium-doped silica-on-silicon [9], polymers [10], lithium niobate [11–13] and so forth. The utmost waveguide width with the single-mode behavior is the optimum condition, because no higher order modes were excited and the fundamental mode had the highest light confinement [14]. Therefore, the single-mode condition in the waveguide should be fulfilled in order to prevent signal distortion during transmission. Many articles have reported the fabrication of microring resonators in LN on insulator [11–13] and simulation of microring resonators in SOI [15,16], but few reports have involved the simulation of single-mode microring resonators in LNOI in the literature so far. Therefore, a search for the simulation and analysis of single-mode microring resonators in LNOI seems to be important. Our work has focused on LNOI-based devices in order to obtain a high Quality Factor (Q-factor) and wide free spectral range (FSR) that are crucial in developing ultra-compact integrations of planar lightwave circuits [4,17,18].

In this paper, we presented results from finite difference time domain (FDTD) numerical simulations. Key optical design parameters of laterally coupled LNOI-based microring resonators were characterized using 2.5-D variational FDTD (varFDTD). Waveguide simulations based on full-vectorial finite difference method were performed by varying the geometrical parameters of waveguide configurations to investigate the single-mode conditions and the propagation losses of LN planar waveguides at different SiO_2 cladding layer thicknesses. In order to obtain an improved wavelength filtering, we performed the optimization for the design parameters which includes ring radii and gap sizes. These parameters affected FSR and Q-factor directly. As a very important element for practical application we described the electro-optical tunable microring resonators on LNOI.

2. Device Description

The material of the device studied in this paper was a z-cut LN thin film stuck to SiO_2 cladding layer deposited on a LN substrate. The schematic of a microring resonator is shown in Figure 1. The modulator consisted of a ring resonator made by the z-cut LN thin film, which was coupled to a channel. If the signal was on-resonance with the ring, then that signal coupled into the cavity from channel. The device parameters such as ring radii and gap sizes between channel and ring resonator were optimized to have the optimum characteristics.

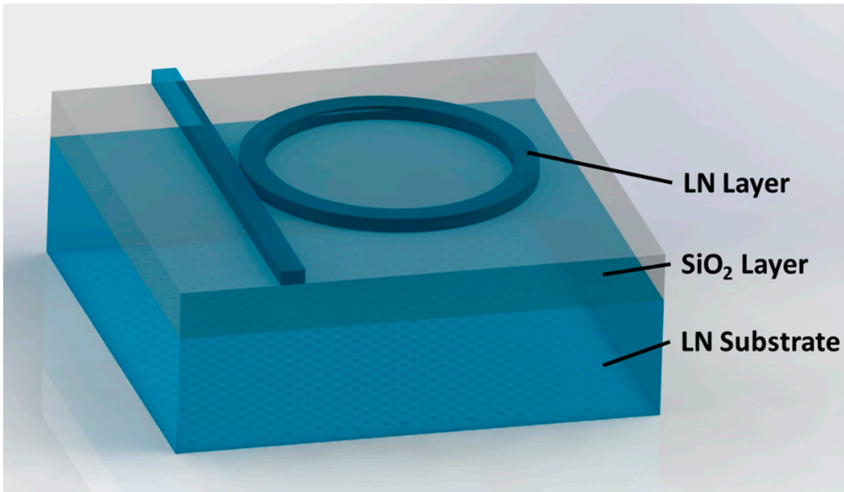

Figure 1. A schematic of the waveguide-coupled microring resonator on LNOI.

The varFDTD method with perfectly matched layers boundary conditions (PML) in this work could show how to design and simulate a microring resonator using the finite difference eigen (FDE) mode solver to achieve a desired FSR and Q factor for a LNOI based. The varFDTD method was a direct time and space solution for solving Maxwell's equations in complex geometries. By performing Fourier transforms, such as the Poynting vector, normalized transmission, and far field projections could be obtained. PML boundaries could absorb electromagnetic energy incident upon them, allowing radiation to propagate out of the computational area without interfering with the field inside [19]. The total ring loss was due to the bend loss and other scattering losses at the coupling region. For the high index contrast wave-guides we were considering, at wavelengths around 1.55 μm, the propagation loss and bend loss were small. For this analysis we would neglect all losses, but the different loss contributions could easily be considered in a more detailed analysis [20].

3. Results and Discussion

The high refractive index difference between the LN (n_o = 2.2129 and n_e = 2.1395 at λ = 1.55 μm) [21] and the SiO_2 (n = 1.46) required the waveguide thickness and the waveguide width to be smaller than a limiting value to achieve single-mode operation. The single mode conditions had been firstly simulated.

We had calculated the modal curves at λ = 1.55 μm for LN ridge waveguides with 0.7 μm width on SiO_2 layer. The effective index dependence on the thickness is presented in Figure 2. The first order mode of the transverse electric (TE) and transverse magnetic (TM) modes appeared at the LN thicknesses of 0.86 μm and 0.84 μm, respectively. To ensure that only one electric field intensity peak was supported in the vertical direction of the LN thin film, the thickness of LN thin film should be less than this critical value. In the following simulation, the thickness of LN thin film was all selected as 0.5 μm.

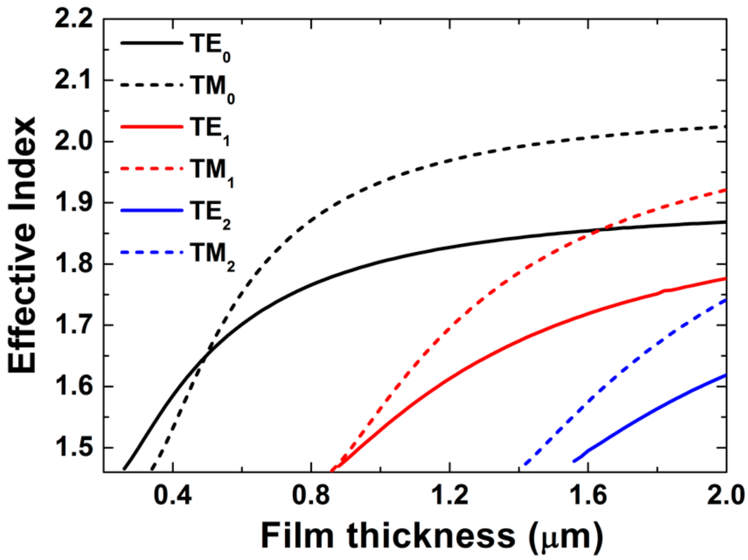

Figure 2. Effective index of the TE (solid lines) and TM (dashed lines) modes in LN waveguides as a function of the film thickness for a waveguide with 0.7 μm width; the modes were calculated at λ = 1.55 μm.

The dependence of the effective index on the waveguide width, assuming a 0.5-μm thick waveguide is shown in Figure 3. The curves showed the boundary between the single-mode and multi-mode conditions. For LN ridge waveguides, the single mode conditions of the TE and TM modes were 1.08 μm and 1.04 μm, respectively. In the following simulations, the widths of LN ridges were all selected as 0.7 μm to ensure that only one mode was supported in the LN thin film.

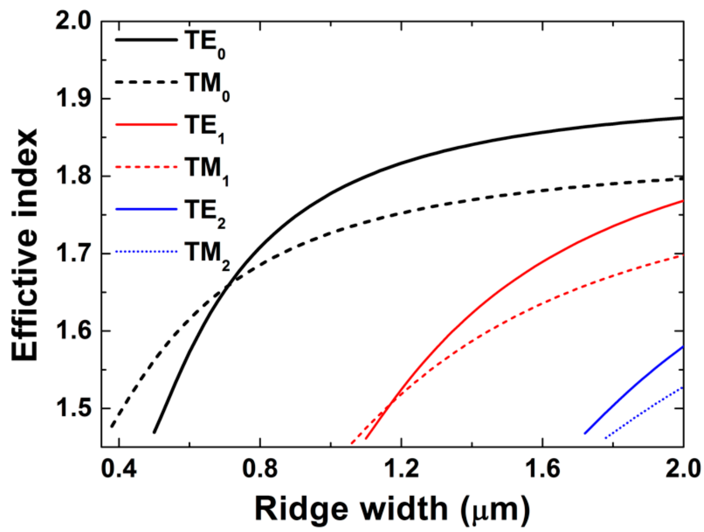

Figure 3. Effective index of the TE (solid lines) and TM (dashed lines) modes in LN waveguides as a function of the width for a 0.5 μm thick film. The modes were calculated at λ = 1.55 μm.

The SiO_2 layer worked as the cladding layer with a thickness of a limiting value, which was sufficiently thick to prevent the field penetration into the bottom layer. The propagation losses of LN planar waveguide with the different SiO_2 layer thicknesses are shown in Figure 4. The propagation losses descended with increasing SiO_2 cladding layer thicknesses. At the same SiO_2 layer thickness, the propagation losses of TE modes were less than those of the TM modes. The diffracted field radiated in the transmission of light, some power was lost into the substrate, but the structure of LN-SiO_2-Au had a metal bottom reflector, the power transmitted to the substrate was reflected by the Au bottom reflector, which resulted a decrease of the propagation losses [22]. The propagation losses of LN-SiO_2-Au were less than those of LN-SiO_2-LN at the same SiO_2 layer thickness. At a SiO_2 layer thickness of 2 μm, the LN planar waveguide losses were all less than 10^{-3} dB/cm, which is negligible. Therefore, the thicknesses of SiO_2 layer were all selected as 2 μm in the following simulation.

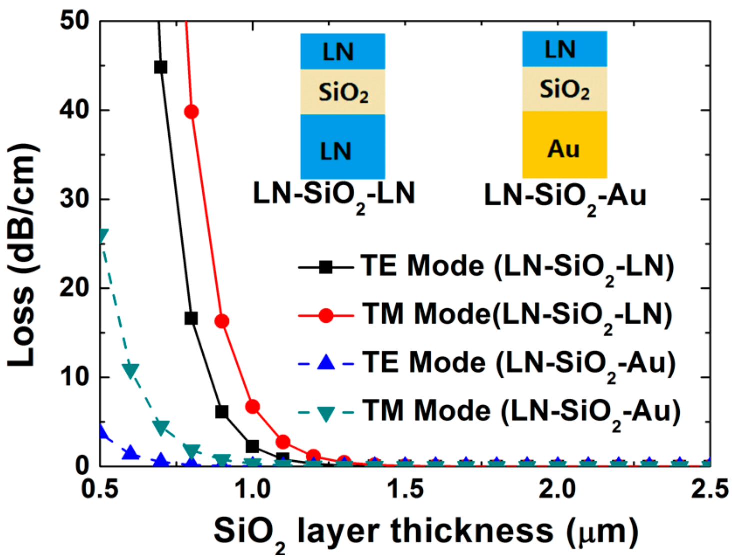

Figure 4. The propagation losses of LN planar waveguide with the different SiO_2 layer thicknesses.

A critical dimension in this optical structure was the gap separating the ring from the tangential waveguide. The gap size determined the input and output couple ratios of the microring resonator, which determined the magnitude of the finesse and the at-resonance transmittance in turn. In the case of a microring coupled to channel, the gaps were very small due to the strong optical confinement and the small coupling interaction length [14].

Because the FSR defined as the separation between two adjacent resonant wavelengths, increased and might become even larger than the wavelength range used for wavelength division multiplex (WDM) applications. However, one of the most critical factors limiting the minimum useful ring radius was the bending loss. These could be qualitatively understood by describing the bend as a straight waveguide, while the effective index was decreasing function in the radial direction. This implied that at a certain distance from the waveguide core, the solution of the Maxwell equations became a radiating field; this radiation was a loss source, as in a leaky waveguide [11].

Using varFDTD, we have calculated Q-factor, bending loss and FSR for a single-mode waveguide at different ring radii and gap sizes (channel and ring width w = 0.7 μm, λ = around 1.55 μm). The results are shown in Figures 5 and 6. According to the Figure 5a, when the radius was smaller than 20 μm, the Q-factor significantly ascended with increased radii, while it was larger than 20 μm, it preserved almost unchangeable values. We also observed that Q-factor ascended with increasing gap sizes and the TE and TM modes showed different results in terms of the achievable Q-factor for this geometry. In the case of gap = 0.29 μm, a Q-factor more than 10,000 was achieved for the TE mode whilst for the TM mode the Q-factor was significantly smaller ~2000. Figure 5b shows Bending loss descended with increasing ring radius, and the bending losses are very low as the radii more than 20 μm. Loss in practical structures would inevitably come up for the following two reasons: on one hand, the scattering by the residual roughness of the etched walls of the photonic wires [17], on the other hand, the modal mismatch at the interface between SiO_2 layer and LN thin film [23]. However, the losses of the LN waveguides could be reduced as much as possible by optimizing the fabrication process of waveguides. At 1590 nm wavelength, the propagation losses of sub-wavelength scale LN waveguides could be as low as 2.7 dB/m by Ar^+ ion etching [12]. As shown in Figure 6, FSR descended with increasing ring radius. Both TE and TM modes achieved the largest FSR for the ring with the smallest radius 3 μm. When the radius was larger than 40 μm and the gap size was 0.1 μm, the FWHM (full-width at half-maximum) of the dip was close to the FSR, the dip became less obvious. Because the effective index of TE mode was larger than that of TM mode, the Q-factor of TE mode was greater than that of TM mode, and FSR of TE mode was less than that of TM mode.

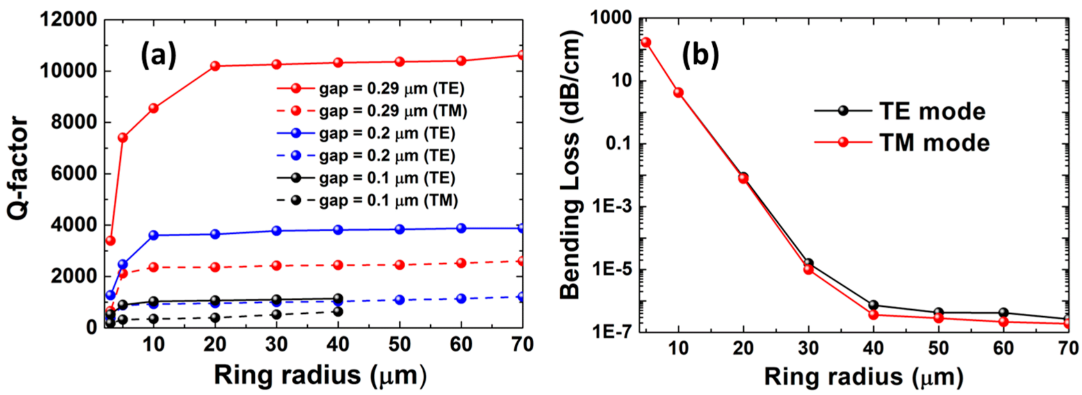

Figure 5. (**a**) Q-factor of microring resonator as different ring radii for different gap sizes, (**b**) Bending loss variation as bending radius. The modes were calculated at λ = around 1.55 μm.

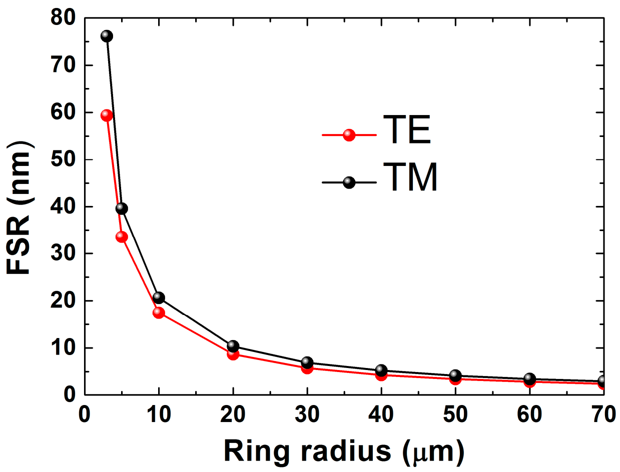

Figure 6. FSR of microring resonators as different ring radii. The modes were calculated at λ = around 1.55 μm.

The electro-optical properties of LN microring resonator have been simulated by applying a static electric field to the device electrodes to shift transmission spectrum. In Figure 7, a LN microring resonator is embedded in the middle of SiO_2 layer, and the electrodes are placed over below and above the SiO_2 layer. A tuning range of microring resonators depend on the strength of the electro-optical effect. However, the electric field achieved in the LN film was relatively weak because the upper and lower cladding materials exhibited one order of magnitude smaller dielectric constants. Due to the large difference between the dielectric constant of the LN thin film (ε_{LN} = 28.5) and the SiO_2 (ε_{SiO_2} = 3.9), the field in the LN thin film was considerably far less than in the SiO_2 layer. The field in the two layers could be calculated from the applied voltage ΔV using the continuity of the vertical component of the electric displacement field D:

$$E_{LN}\, d_{LN} + E_{SiO_2}\, d_{SiO_2} = \Delta V, \tag{1}$$

$$D = \varepsilon_0\, \varepsilon_{LN}\, E_{LN} = \varepsilon_0\, \varepsilon_{SiO_2}\, E_{SiO_2} = \text{const}, \tag{2}$$

d_{LN} and d_{SiO_2} were the thicknesses of LN thin film and SiO_2 layer, which have been determined. Therefore, the electric field in the LN thin film layer is given by Equations (1) and (2).

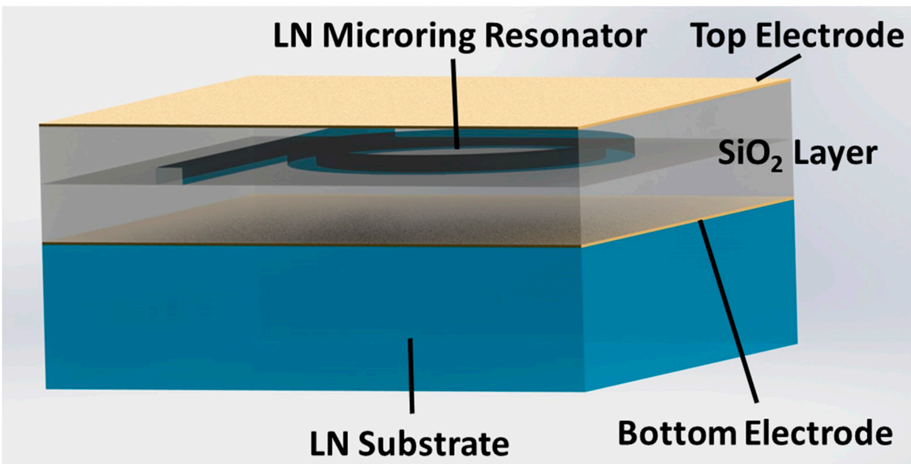

Figure 7. The LN microring resonator was embedded in the middle SiO_2 layer, and the electrodes were placed over below and above the SiO_2 layer.

Optical transmission simulations were performed to characterize the electrical tuning of optical resonances. To observe the electro-optic effect, an electric field applied between the top and the bottom electrodes by applying different direct current (DC) voltages was considered uniform. Figure 8 shows the simulated TM-mode spectrum as a function of different electric field intensities. The resonance wavelength shifted ascending with increasingly electric field intensity. The resonance shifts were 99 pm, 198 pm, 297 pm, and 395 pm for the chance in different electric field intensities from 0 V/μm to 1 V/μm, 2 V/μm, 3 V/μm, and 4 V/μm, respectively.

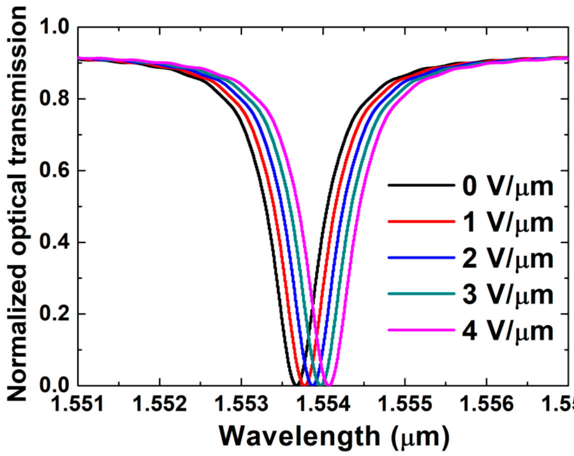

Figure 8. Transmission spectra of wavelength shift due to different electric field intensities in the Z-direction. The calculations referred to the TM mode at the microring radius R = 20 μm.

4. Conclusions

In conclusion, a VarFDTD method was used to design and simulate various waveguides and waveguide-coupled single-mode microring resonators in z-cut LNOI. Single mode conditions were obtained. The propagation losses of LN planar waveguides were calculated by full-vectorial finite difference method. The propagation losses of LN planar waveguides decreased with the increase of the SiO_2 cladding layer thickness. The thickness of LN Film, width of ridge waveguide and thickness of SiO_2 layer were optimized to 0.5 μm, 0.7 μm and 2 μm, respectively. Q-factor ascended with increasing radius and gap sizes, while FSR descended with increasing radius. A microring resonator with Q-factor more than 10,000 and FSR more than 8 nm was achieved in the case of gap = 0.29 μm and radius R = 20 μm. Our simulation showed that the resonance wavelength of the electro-optical microresonators in LNOI shifted ascending with increasingly electric field intensity. This work will continue with fabrication and characterization. For this purpose, the results provided here will be of useful guidance before laboratory works are carried out.

Author Contributions: B.X. conceived the original idea; H.H. carried out the simulations, analyzed the data, and wrote the paper; B.X. and J.Z. contributed the useful and deep discussions and modified the manuscript.

Funding: This work was supported by the National Natural Science Foundation of China (NSFC) (Grants NO. 61701288), the Shenzhen Science and Technology Planning (NO. JCYJ20170818143327496), the Foundation of Zibo Vocational Institute (NO. 2018zzzr03), and the Shandong University Science and Technology Planning (NO. J16LN93).

Conflicts of Interest: The authors declare no conflict of interest.

References

1. Weis, R.S.; Gaylord, T.K. Lithium niobate: Summary of physical properties and crystal structure. *Appl. Phys. A* **1985**, *37*, 191–203. [CrossRef]
2. Chen, L.; Wood, M.G.; Reano, R.M. 12.5 pm/V hybrid silicon and lithium niobate optical microring resonator with integrated electrodes. *Opt. Express* **2013**, *21*, 27003–27010. [CrossRef] [PubMed]

3. Rabiei, P.; Gunter, P. Optical and electro-optical properties of submicrometer lithium niobate slab waveguides prepared by crystal ion slicing and wafer bonding. *Appl. Phys. Lett.* **2004**, *85*, 4603–4605. [CrossRef]
4. Poberaj, G.; Hu, H.; Sohler, W.; Günter, P. Lithium niobate on insulator (LNOI) for micro-photonic devices. *Laser Photon. Rev.* **2012**, *6*, 488–503. [CrossRef]
5. Tao, S.H.; Mao, S.C.; Song, J.F.; Fang, Q.; Yu, M.B.; Lo, G.Q.; Kwong, D.L. Ultra-high order ring resonator system with sharp transmission peaks. *Opt. Express* **2010**, *18*, 393–400. [CrossRef] [PubMed]
6. Rafizadeh, D.; Zhang, J.P.; Hagness, S.C.; Taflove, A.; Stair, K.A.; Ho, S.T.; Tiberio, R.C. Waveguide-coupled AlGaAs/GaAs microcavity ring and disk resonators with high finesse and 21.6-nm free spectral range. *Opt. Lett.* **1997**, *22*, 1244–1246. [CrossRef] [PubMed]
7. Rao, A.; Fathpour, S. Compact lithium niobate electrooptic modulators. *IEEE J. Sel. Top. Quantum Elect.* **2018**, *24*, 1–14. [CrossRef]
8. Almeida, V.R.; Barrios, C.A.; Panepucci, R.R.; Lipson, M. All-optical control of light on a silicon chip. *Nature* **2004**, *431*, 1081–1084. [CrossRef] [PubMed]
9. Shahoei, H.; Dumais, P.; Yao, J. Continuously tunable photonic fractional Hilbert transformer using a high-contrast germanium-doped silica-on-silicon microring resonator. *Opt. Lett.* **2014**, *39*, 2778–2781. [CrossRef] [PubMed]
10. Rabiei, P.; Steier, W.H.; Zhang, C.; Dalton, L.R. Polymer micro-ring filters and modulators. *J. Lightwave Technol.* **2002**, *20*, 1968–1975. [CrossRef]
11. Guarino, A.; Poberaj, G.; Rezzonico, D.; Degl'innocenti, R.; Günter, P. Electro-optically tunable microring resonators in lithium niobate. *Nat. Photon.* **2007**, *1*, 407–410. [CrossRef]
12. Zhang, M.; Wang, C.; Cheng, R.; Shams-Ansari, A.; Lončar, M. Monolithic ultra-high-Q lithium niobate microring resonator. *Optica* **2017**, *4*, 1536–1537. [CrossRef]
13. Siew, S.Y.; Saha, S.S.; Tsang, M.; Danner, A.J. Rib microring resonators in lithium niobate on insulator. *IEEE Photon. Technol. Lett.* **2016**, *28*, 573–576. [CrossRef]
14. Chin, M.K.; Ho, S.T. Design and modeling of waveguide-coupled single-mode microring resonators. *J. Lightwave Technol.* **1998**, *16*, 1433–1446. [CrossRef]
15. Lalanne, P.; Hugonin, J.P. Bloch-wave engineering for high-Q, small-V microcavities. *IEEE J. Sel. Top. Quantum Elect.* **2003**, *39*, 1430–1438. [CrossRef]
16. Hazura, H.; Shaari, S.; Menon, P.S.; Majlis, B.Y.; Mardiana, B.; Hanim, A.R. Design parameters investigation of single mode silicon-on-insulator (SOI) microring channel dropping filter. *Adv. Sci. Lett.* **2013**, *19*, 199–202. [CrossRef]
17. Hu, H.; Yang, J.; Gui, L.; Sohler, W. Lithium niobate-on-insulator (LNOI): Status and perspectives. *Proc. SPIE.* **2012**, *8431*, 84311D.
18. Rao, A.; Fathpour, S. Heterogeneous thin-film lithium niobate integrated photonics for electrooptics and nonlinear optics. *IEEE J. Sel. Top. Quantum Elect.* **2018**, *24*, 8200912. [CrossRef]
19. Chen, Z.; Wang, Y.; Jiang, Y.; Kong, R.; Hu, H. Grating coupler on single-crystal lithium niobate thin film. *Opt. Mater.* **2017**, *72*, 136–139. [CrossRef]
20. Lumerical Solutions. Available online: http://www.lumerical.com/ (accessed on 4 August 2018).
21. Schlarb, U.; Betzler, K. A generalized sellmeier equation for the refractive indices of lithium niobate. *Ferroelectrics* **1994**, *156*, 99–104. [CrossRef]
22. Chen, Z.; Peng, R.; Wang, Y.; Zhu, H.; Hu, H. Grating coupler on lithium niobate thin film waveguide with a metal bottom reflector. *Opt. Mater. Express* **2017**, *7*, 4010–4017. [CrossRef]
23. Han, H.; Cai, L.; Xiang, B.; Jiang, Y.; Hu, H. Lithium-rich vapor transport equilibration in single-crystal lithium niobate thin film at low temperature. *Opt. Mater. Express* **2015**, *5*, 2634–2641. [CrossRef]